Research Square

Preprints are preliminary reports that have not undergone peer review.
They should not be considered conclusive, used to inform clinical practice,
or referenced by the media as validated information.

A preliminary study on the ultrasonic manifestations of peripulmonary lesions of non-critical novel coronavirus pneumonia (COVID-19)

Yi Huang
Department of Ultrasound, Xi'an Chest Hospital, Xi'an, 710100, China
Sihan Wang
Yue Liu
Yaohui Zhang
Chuyun Zheng
Yu Zheng
Chaoyang Zhang
Weili Min
Ming Yu (mingyu@fmmu.edu.cn)
Department of Ultrasound, Xijing Hospital, Airforce Medical University, Xi'an, 710032, China.
Mingjun Hu (763422088@qq.com)
Department of Ultrasound, Xi'an Chest Hospital, Xi'an, 710100, China

Research Article

Keywords: lung ultrasound, ultrasonic manifestations, novel coronavirus pneumonia (COVID-19)

Posted Date: February 26th, 2020

DOI: https://doi.org/10.21203/rs.2.24369/v1

License: This work is licensed under a Creative Commons Attribution 4.0 International License.
Read Full License

Abstract

Background:

Ultrasound is used to observe the imaging manifestations of COVID-19 in order to provide reference for real-time bedside evaluation.

Purpose: To explore the ultrasonic manifestations of peripulmonary lesions of non-critical COVID-19, so as to provide reference for clinical diagnosis and efficacy evaluation.

Materials and Methods: The clinical and ultrasonic data of 20 patients with clinically diagnosed non-critical COVID-19 treated in Xi'an Chest Hospital during January and February 2020 were retrospectively analyzed. Conventional two-dimensional ultrasound and color Doppler ultrasound were used to observe the characteristics of lesions.

Results: All 20 patients (40 lungs and 240 lung areas) had a history of travel, residence or close contact in/with Wuhan, and 5 of them caught COVID-19 after family gatherings. Lesions tended to occur in both lungs. Lesions in the lung areas: 14 in L1+R1 area (14/40), 17 in L2+R2 area (17/40), 17 in L3+R3 area (17/40), 17 in L4+R4 area (17/40), 20 in L5+R5 area (20/40), and 28 in L6+R6 area (28/40). Lesion types: rough and discontinuous pleural line (36/240), subpleural consolidation (53/240), air bronchogram sign or air bronchiologram sign in subpleural peripleural consolidation (37/240), visible B lines (91/240), localized pleural thickening (19/240), localized pleural effusion (24/240), poor blood flow in the consolidation detected by color Doppler ultrasound (50/53).

Conclusion: The non-critical COVID-19 has characteristic ultrasonic manifestations, which are visible in the posterior and inferior areas of the lung. The lesions are mainly characterized by a large number of B lines, subpleural pulmonary consolidation and poor blood flow. Lung ultrasound can provide reference for the clinical diagnosis and efficacy evaluation.

Chinese Clinical Trial Registry: ChiCTR2000030032

Approval for Scientific Research Project: No. 2020-S0001

Summary Statement

With reference to the *Diagnosis and Treatment Protocols of COVID–19* (trail version 6), COVID–19 is classified as mild, usual, severe and critical. Non-critical COVID–19 refers to mild, usual and severe COVID–19. The examination time is 0–10 days after onset.

Key Results

1. COVID–19 foci are mainly observed in the posterior fields in both lungs, especially in the posterior lower fields.

2. Fused B lines and waterfall signs are visible under the pleura. The B lines are in fixed position.
3. The pleural line is unsmooth, discontinuous and interrupted.
4. The subpleural lesions show patchy, strip, and nodule consolidation.
5. Air bronchogram sign or air bronchiologram sign can be seen in the consolidation.
6. The involved interstitial tissues have localized thickening and edema, and there is localized pleural effusion around the lesions.
7. CDFI ultrasound shows insufficient blood supply in the lesions.
8. High frequency linear array probe is suggested to be used for minor subpleural lesions, as it can provide rich information and improve diagnostic accuracy.

Introduction

As reported on February 14, 2020, the outbreak of COVID–19 in China has currently caused 55,748 confirmed cases, 6,723 suspected cases, and 1,380 deaths in 31 provinces (autonomous regions and municipalities) and Xinjiang, with a total of 63,851 accumulated confirmed cases [1–3]. Confirmed cases have also been reported in other countries [4]. On January 30, 2020, WHO defined this epidemic as a public health emergency of international concern (PHEIC). In addition to routine blood tests and real-time fluorescent RT-PCR, imaging diagnosis, especially CT, is playing an irreplaceable role [2,5,6]. However, CT has certain disadvantages as the equipment is insufficient and hard to move, and may cause cross infections. The average diameter of SARS-CoV–2 is about 120nm, so it is speculated that the virus particles can be inhaled into the airway and lungs, even into the alveoli. This may explain why the lesions of viral pneumonia are mainly in the subpleural areas. What has been clear is that COVID–19 generally begins in the terminal alveoli, which are close to the pleura and can be clearly observed by lung ultrasound. No reports on the ultrasonic findings of COVID–19 have been retrieved so far, so this paper hopes to provide preliminary ultrasonic information of COVID–19. What is more important, in clinical practice, for patients who cannot be moved or who cannot receive radiographic examination, in case the disease progresses rapidly, timely bedside evaluation is crucial to adjust the treatment plan.

Clinical lung ultrasound has been developed for many years and is now a mature practice. Its application in the diagnosis of severe lung diseases has received considerable recognition [7.8]. The authors retrieved relevant literature [2,5,9–11], but found no domestic or foreign studies or reports on the ultrasonic imaging manifestations of non-critical COVID–19. This study retrospectively analyzed the color Doppler ultrasound information of peripulmonary lesions of early and progressive COVID–19 in 20 patients treated in Designated Hospital, hoping to provide real-time reference for the clinical diagnosis, treatment, and efficacy evaluation of the disease, solve problems caused by reliance on large, stationary CT, and provide evidence-based literature.

Materials And Methods

Patients

A total of 20 COVID–19 cases treated during January and February 2020 in the Emergency Respiratory Department of Designated Hospital were involved. With reference to the *Diagnosis and Treatment Protocols of COVID–19* (trail version 5) formulated by National Health Commission of the People's Republic of China, all patients enrolled met the following requirements: 1. Epidemiological history: 1) Travel/residence history in Wuhan or other areas with COVID–19 transmission within 14 days prior to onset of illness; 2) Exposure to patients with fever or respiratory symptoms who were from Wuhan or other areas with COVID–19 transmission within 14 days prior to the onset of disease; 3) Clusters or epidemiological associations with COVID–19 infections. 2. Clinical manifestations: 1) fever; 2) Radiographic features of pneumonia with ground glass opacity or patchy consolidation in the lungs; 3) Normal or decreased number of white blood cells, decreased lymphocyte count in the early stage of disease. 3. Blood or respiratory specimens: 1) Positive nucleic acid of SARS-CoV–2 detected by real-time fluorescence RT-PCR; 2) Highly homologous virus gene sequencing with SARS-CoV–2. Patients enrolled in the study met the above criteria and were clinically diagnosed as non-critical patients. This study was approved by the Ethics Committee of Xi'an Chest Hospital, and all patients recruited signed the informed consent to publication of their personal medical records.

Equipment

SonoScape P50 color ultrasonic device was used. The frequency was 1–8 MHz for convex array probe and 3–17 MHz for linear array probe. Film and 75% alcohol were used to protect and disinfect the device.

Operational procedures

The 12-area examination method was adopted, in which a lung was divided by the anterior axillary and posterior axillary lines into 3 areas: anterior, lateral and posterior. The 2 lungs were divided into 6 areas. To avoid errors, the blue dots in Bedside Lung Ultrasound in Emergency-PLUS (BLUE-PLUS) served as the boundary, and were perpendicularly connected with the axillary anterior and posterior lines to the spine point to divide each lung into upper and lower fields. As a result, the 2 lungs were divided into 12 areas. In order to mark and describe the lesion sites clearly, R/L1□6 subdivision labeling method was used. R represented the right lung (R1: right anterior upper area; R2: right anterior lower area; R3: right axillary upper area; R4: right axillary lower area; R5: right posterior upper area; R6: right posterior lower area). L represented the left lung (L1: left anterior upper area; L2: left anterior lower area; L3: left axillary upper area; L4: left axillary lower area; L5: left posterior upper area; L6: left posterior lower area). Observations included: whether the pleural line was smooth, continuous or interrupted; the distribution, number and fusion of B lines in the peripulmonary area of both lungs; the echo, location, shape and range of peripulmonary lesions; whether there was air bronchogram sign or air bronchiologram sign in the

consolidation; blood flow in the consolidation; whether there was pleural effusion around the lesions or localized pleural thickening.

Imaging analysis

The images of different areas of lungs were examined one after another. The areas with obvious features of lesions, surrounding lung tissues and chest wall tissues were selected as the areas of interest. The above evaluations were performed by 2 physicians with more than 5 years of experience in ultrasound.

Statistical Analysis

Statistical analysis was conducted with SPSS22.0, the ratio was expressed with 95%CI, and the plot was drawn with MedCale.

Results

General Information

Altogether 20 cases were enrolled, including 11 male and 9 female, average age 27–81 years, median 44.5 years (3 cases ≥65 years, 17 cases < 65 years). If a case had multiple lesions in both lungs, the largest lesion was selected for observation. Lung ultrasound examined the 6 lung fields and 12 lung areas in all patients. The number of lesions were shown in Diagram 1.

Analysis of the lesion types at various sites showed the proportion of B lines was higher in the lesions than in other areas (95%CI: 0.317–0.441). The blood flow signs were fewer in the lesions than in other areas (95%CI: 0.008–0.121).

Diagram 2 General information and ultrasonic manifestations of COVID–19

Discussion

Different from previous pneumonia transmissions caused by influenza virus [3,10,12], COVID–19 is characterized by rapid transmission, high infection rate and high lethality. In addition to chest X-ray and CT scan, ultrasound can also be used for the diagnosis and treatment. It has been confirmed that COVID–19 can be transmitted by droplets and direct contact; therefore, ultrasonic device has advantages over CT and DR in disinfection and smaller area of contact with patients. In particular, 9–15 MHz high-frequency linear array probe can clearly display the morphology and changes of subpleural lesions, and the changes of air and water contents in consolidated peripulmonary tissues [6.13]. It has been reported that 3–17 MHz high-frequency linear array probe can show air bronchogram sign in unconsolidated lung tissues caused by intra-pulmonary hemorrhage [14], which is of great significance for the close

observation of peripulmonary lesions. Color flow Doppler technique can show the blood supply and lesion progression in peripulmonary consolidation, which has special clinical significance [15]. Therefore, ultrasound is playing an indispensable role in the diagnosis, treatment and efficacy evaluation of severe acute pneumonia [7,16].

Since few studies investigated the ultrasonic manifestations of non-critical COVID–19 [2.3.9–12], this study focuses on the ultrasonic manifestations and characteristics and their relationship with CT images. Currently, ultrasound is largely limited in the diagnosis and treatment of central lung diseases and bone-occlusion lung diseases due to the attenuation of sound waves by normal lung and bone tissues. Therefore, lung ultrasound relies on the artifacts of peripulmonary lesions to make the diagnosis [17,18], while the artifacts occur because of the abnormal sound wave reflection caused by changes in the ratio of air and water contents in alveoli and interstitial tissues due to peripulmonary lesions. Based on this speculation, this study used abdominal convex array ultrasound combined with 3–17 MHz high frequency linear array probe to observe the pulmonary lesions and artifacts. The authors believed that B lines emerged mainly because in the COVID–19 cases enrolled, most of the lesions were observed under the peripulmonary pleura, which resulted in the thickening and edema of interstitial tissues, reduced air content in alveoli, and artifacts caused by ultrasonic ringing effects.

Ultrasound images showed that the subpleural lesions in the course of non-critical COVID–19 were significantly different from other lesions reported in literature [8,17], such as bacterial pneumonia, pulmonary abscess, tuberculosis, compression and obstructive atelectasis, pneumothorax, benign and malignant tumors, and so on. Lung ultrasound revealed the following radiographic features of non-critical COVID–19:

Lesions were mostly located in the posterior fields of both lungs. Multiple discontinuous or continuous fused B lines (waterfall sign) under the pleural line were visible as shown in Figure 2, or diffused B lines (white lung sign), and the A lines disappeared as shown in Figure 4. Compared with the B lines caused by cardiogenic pulmonary edema, the B lines here were more likely to be fused and fixed. The B lines had blurred edges and no bifurcation signs. The origination point of the subpleural lesion was more obtuse (convex array probe) compared with that of B lines of pulmonary edema, as shown in Figure 6.

High frequency ultrasound showed that the pleural line was unsmooth and rough, as shown in Figure 8 and 10, and interrupted as shown in Figure 12, mainly due to the decreased gas content and sound wave reflection in the subpleural alveoli and interstitial lesions.

Multiple small patchy consolidations were observed in the subpleural lesion, as shown in Figure 13, and strip consolidation was shown in Figure 16.

The echogenicity in the lesions was homogeneous or inhomogeneous, and air bronchiologram sign was visible (mostly early and progressive stages as shown in Figure 19, because secondary pulmonary lobules were involved by interstitial inflammation, the interstitial tissues were thickened and swollen,

some bronchioles and alveoli were not involved by high gas content) or air bronchogram sign (visible in severe cases or local consolidation, possibly because local inflammation storm caused the consolidation and edema of most bronchioles and alveoli, and only large bronchi and part of the alveoli were not involved, as shown in Figure 20, 21, 22), diffuse B lines. Some patients had long onset and the symptoms improved, then CT images showed nodule consolidation, and ultrasound showed irregular nodule subpleural echo shadow, with fused B lines in fixed position, as shown in Figure 23.

High frequency ultrasound also showed the localized pleural thickening and local pleural effusion around the subpleural lesion. Linear array probe clearly showed that most patients' pleural thickening was about 1–2mm, and the subpleural effusion was about 2–3mm, which changed with the progress of disease, as shown in Figure 24.

CDFI ultrasound showed insensitivity of blood flow signals in subpleural consolidation as shown in Figure 13 and 25. Although ultrasonic devices of different brands were used, the signal of blood flow was still poor, possibly due to the pathological nature and progression of lesions. Great attention should be paid to this, because pulmonary consolidation caused by common inflammation generally shows abundant blood flow signals and the prognosis is good, but COVID–19 progresses rapidly and may cause death. Whether lung tissues are unable to quickly establish microvessel exchange mechanism has yet to be further studied, but color Doppler ultrasound, compared with other medical equipment, can more effectively detect the blood supply in consolidation, and therefore is more useful for clinicians to prejudge the prognosis and process of the disease.

Comparing CT images and ultrasound images of patients with non-critical COVID–19, we can find that the two types of images were highly consistent, but CT showed more clear and complete intrapulmonary and apical lesions than ultrasound. Meanwhile, ground glass opacity, nodule shadow, consolidation shadow and air bronchogram sign all had special manifestations in ultrasonic images as shown in Figure 1, 3, 5, 7, 9, 11, 14, 15, 17, 18, 20 and 21. However, CT is inferior to ultrasound in showing the smaller peripulmonary lesions and pleural and peripulmonary effusion. On the other hand, ultrasound can produce real-time and dynamic images, and is therefore more advantageous in distinguishing interstitial lesions and showing the distribution of blood flow and angiogenesis in inflammatory lesions.

In summary, the COVID–19 foci are mainly observed in the posterior fields in both lungs, especially the posterior and inferior fields. Fused B lines and waterfall signs are visible. The pleural line is unsmooth, discontinuous or interrupted. The subpleural lesions show patchy, strip, and nodule consolidation, in which air bronchogram sign or air bronchiologram sign can be seen. The involved interstitial tissues show obvious thickening and edema, the pleura shows localized thickening, and there is localized pleural effusion around the lesions. CDFI ultrasound shows insufficient blood supply in the lesions. High frequency linear array probe is suggested to be used for minor subpleural lesions, for it can provide rich information and improve the diagnostic accuracy. Our study indicated that ultrasound can show typical manifestations and has advantages over CT in the clinical diagnosis and treatment of non-critical COVID–19, but it cannot replace CT. Ultrasound can be used as a supplementary method. This study has

some limitations: the sample size is small, the changes of ultrasonic images are not carefully examined, and no control studies are conducted. Further large sample studies remain to be conducted.

References

1. Li Q, Guan X, Wu P, et al. Early transmission dynamics in Wuhan, China, of novel coronavirus-infected pneumonia. N Engl J Med 2020. DOI:10.1056/NEJMoa2001316.
2. National Health Commission of the People's Republic of China. Diagnosis and Treatment Protocols of COVID–19 (trail version 5) [EB/OL]. [2020–02–05]. http://www.nhc.gov.cn/xcs/zhengcwj/202002/3b09b894ac9b4204a79db5b8912d4440.shtml.
3. World Health Organization. Clinical management of severe acute respiratory infection when novel coronavirus (nCoV) infection is suspected, interim guidance [EB/OL]. [2020–01–13]. https://www.who.int/publications-detail/clinical-management-of-severe-acute-respiratory-infection-when-novel-coronavirus-(ncov)-infection-is-suspected.
4. Rothe C, Schunk M, Sothmann P, et al. Transmission of 2019-nCoV infection from an asymptomatic contact in Germany. N Engl J Med 2020. DOI:10.1056/NEJMc2001468.
5. World Health Organization. Infection prevention and control during health care when novel coronavirus (nCoV) infection is suspected, interim guidance [EB/OL]. [2020–01–15]. https://www.who.int/internal-publications-detail/surveillance-case-definitions-for-human-infection-withnovel-coronavirus-(ncov).
6. Lei J, Li J, Li X, et al. CT Imaging of the 2019 Novel Coronavirus (2019-nCoV) Pneumonia. Radiology 2020; 31: 200236. doi:10.1148/radiol.2020200236. [Epub ahead of print].
7. Xirouchaki N, Kondili E, Prinianakis G, et al. Impact of lung ultrasound on clinical decision making in critically ill patients. Intensive Care Med 2014; 40(I): 57–65.
8. Wang XT, Liu Dw, Yu KJ, et al. Consensus on severe diseases from Chinese ultrasound experts. Clinical Focus 2017; 5(32): 369–383.
9. Huang C, Wang Y, Li X, et al. Clinical features of patients infected with 2019 novel coronavirus in Wuhan, China. Lancet 2020. DOI: 10.1016/S0140–6736(20)30183–5.
10. Chan JF, Yuan S, Kok KH, et al. A familial cluster of pneumonia associated with the 2019 novel coronavirus indicating person-to-person transmission: a study of a family cluster. Lancet 2020. DOI: 10.1016/S0140–6736(20)30154–9.
11. Ren LL, Wang YM, Wu ZQ. et al. Identification of a novel coronavirus causing severe pneumonia in human: a descriptive study. Chin Med J (Engl) 2020, 30. doi: 10.1097/CM9.0000000000000722. [Epub ahead of print].
12. Wang W, Tang J, Wei F. Updated understanding of the outbreak of 2019 novel coronavirus (2019.nCoV) in Wuhan, China. J Med Virol 2020. Jan 29. doi:10.1002/jmv.25689.[Epub ahead of print].

13. Wang G. Ji X, Xu Y, et al, Lung ultrasound: a promising tool to monitor ventilator-associated pneumonia in critically ill patients. Crit Care 2016; 20(1): 320.
14. Diffuse alveolar hemorrhage in pulmonary ultrasound. Ultrasound Quarterly 2017; 33(1):86–89.doi:10.1097/RUQ.0000000000000259.
15. Yin W, Li Y, Zeng X, et al. The utilization of critical care ultrasound to assess hemodynamics and lung pathology on ICU admission and the potential for predicting outcome. PLoS One 2017; 12(8): e0182881.
16. Yang Y, Wang Z, et al. Application of pulmonary ultrasound in severe H7N9. Chinese Journal of Medical Ultrasound (Electronic Edition) 2019; 16(01): 72–76.
17. Liu J, Feng X, et al. New guidelines for ultrasonic diagnosis of neonatal lung diseases. Chinese Journal of Contemporary Pediatrics 2019; 21(02):105–113.
18. Leech M, Bissett B, Kot M, et al. Lung ultrasound for critical care physiotherapists: a narrative review. Physiother Res Int 2015; 20(2): 69–76.

Figures

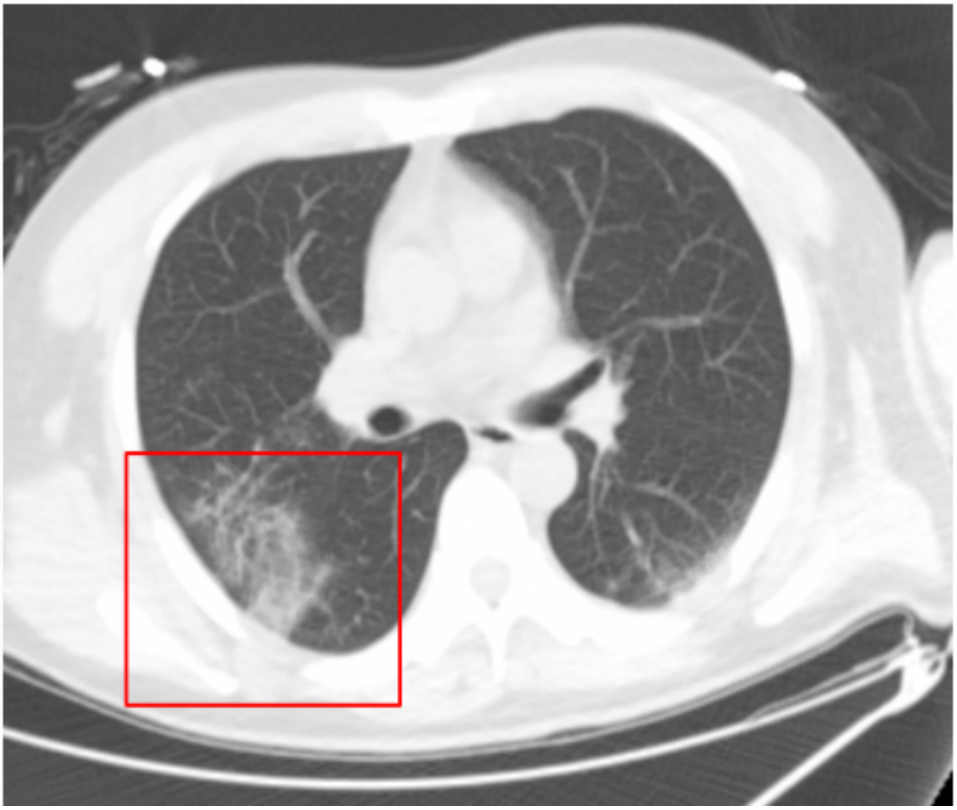

Figure 1

Figure 1 & 2: The same patient. HRCT showed ground glass opacity and air bronchogram sign under the pleura in the posterior upper field of the right lung. The convex array probe showed B lines and waterfall sign in the right posterior upper area (red arrow), and the pleural line was unsmooth.

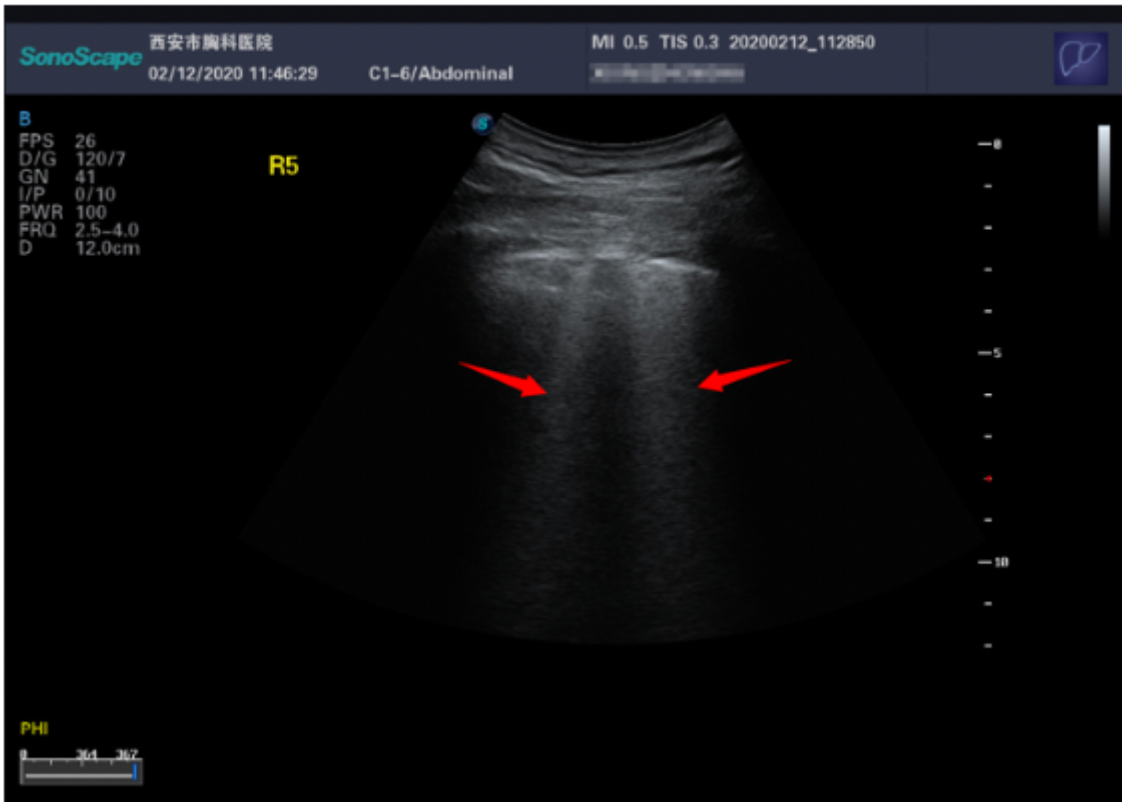

Figure 2

Figure 1 & 2: The same patient. HRCT showed ground glass opacity and air bronchogram sign under the pleura in the posterior upper field of the right lung. The convex array probe showed B lines and waterfall sign in the right posterior upper area (red arrow), and the pleural line was unsmooth.

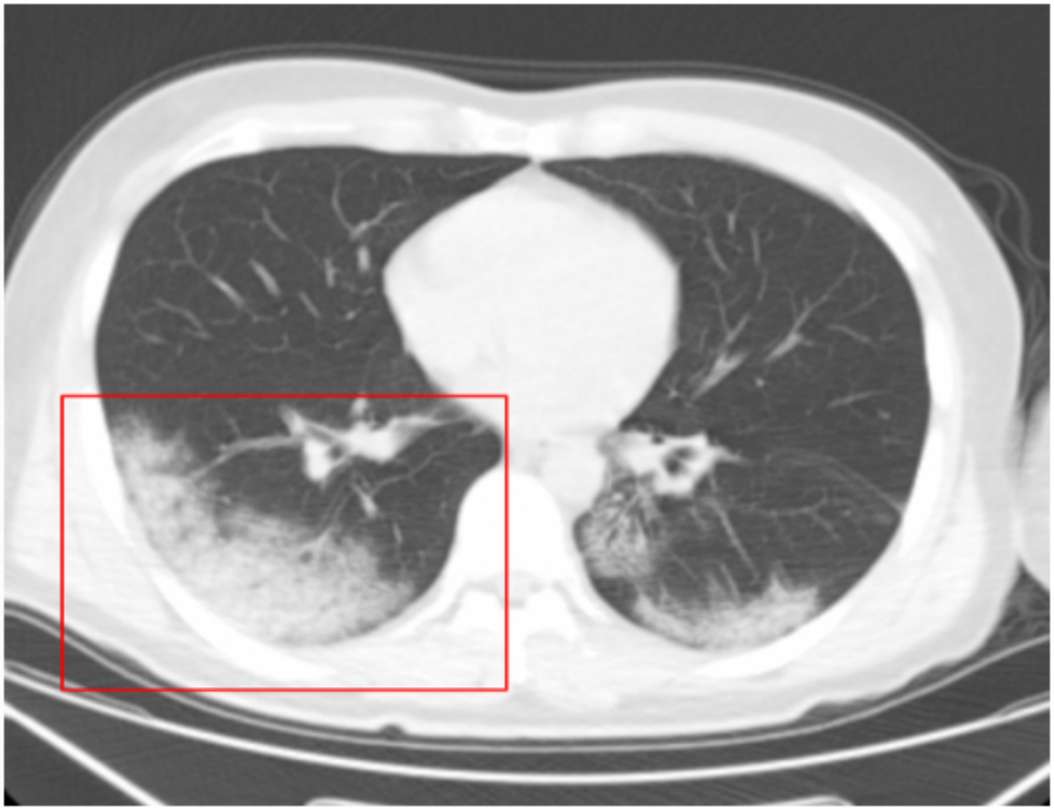

Figure 3

Figure 3 & 4: The same patient. HRCT showed ground glass opacity, cloudy shadows under the pleura in the posterior lower field of the right lung, air bronchogram sign and air bronchiologram sign. The linear array probe showed the pleural line in the right posterior lower area was unsmooth, with crazy-paving pattern, and the roughness was discontinuous. The convex array probe showed the pleural line in the right posterior lower area was unsmooth and thin with diffused B lines and “white lung" sign. A lines disappeared.

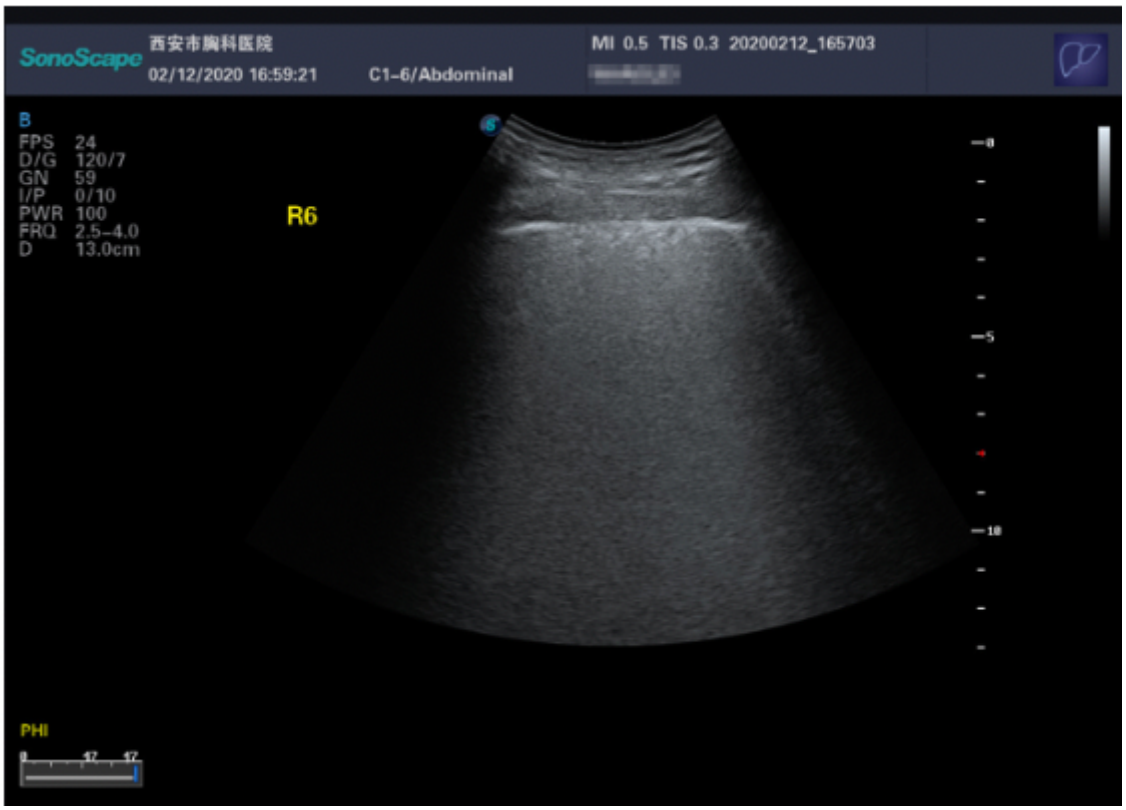

Figure 4

Figure 3 & 4: The same patient. HRCT showed ground glass opacity, cloudy shadows under the pleura in the posterior lower field of the right lung, air bronchogram sign and air bronchiologram sign. The linear array probe showed the pleural line in the right posterior lower area was unsmooth, with crazy-paving pattern, and the roughness was discontinuous. The convex array probe showed the pleural line in the right posterior lower area was unsmooth and thin with diffused B lines and “white lung" sign. A lines disappeared.

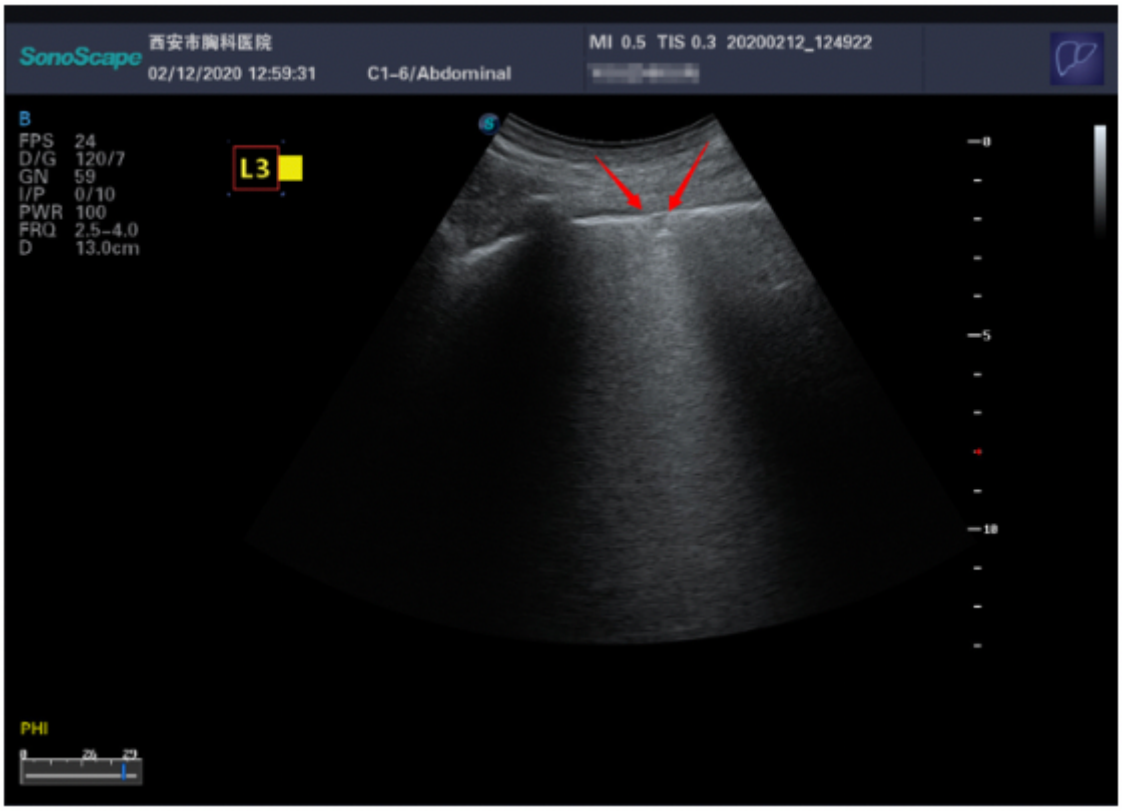

Figure 5

Figure 5 & 6: The same patient. HRCT showed ground glass opacity and reticular shadows under the pleura in the field of the left lung. The convex array probe revealed B lines in the left posterior lower area and A lines disappeared. Small patchy lesions were observed, and the pleural line was discontinuous (red arrow).

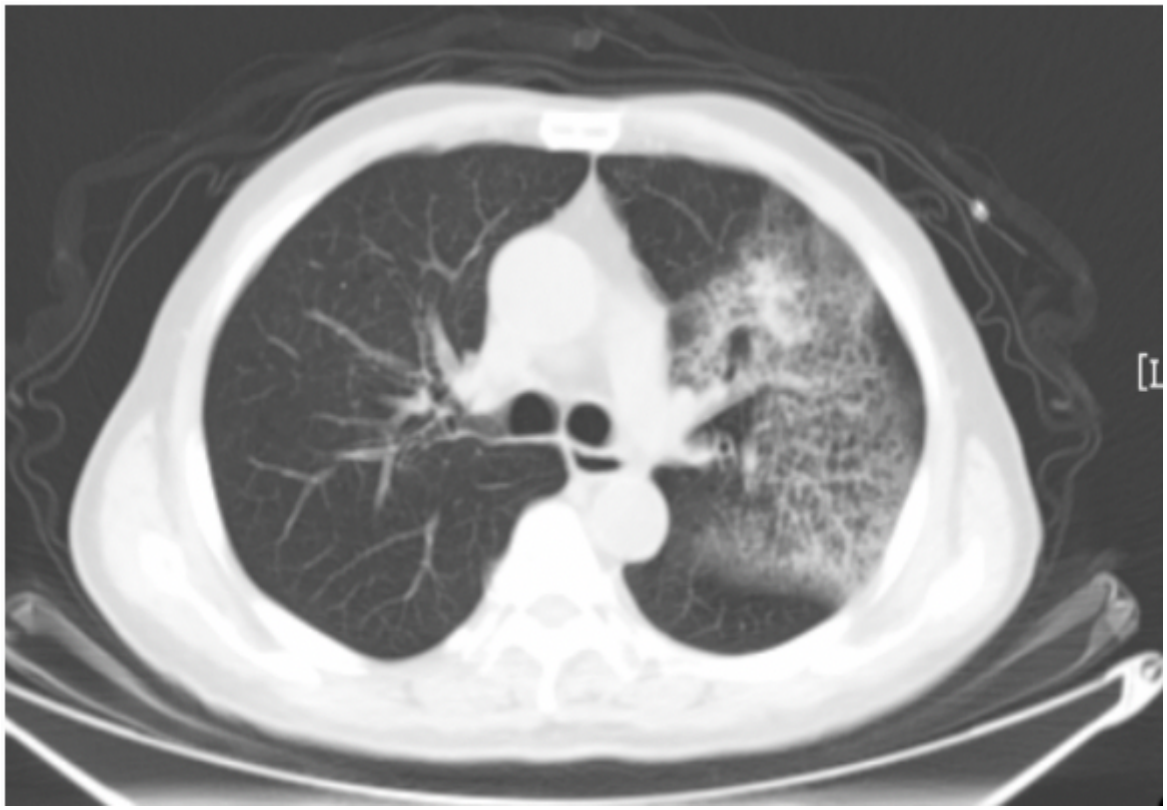

Figure 6

Figure 5 & 6: The same patient. HRCT showed ground glass opacity and reticular shadows under the pleura in the field of the left lung. The convex array probe revealed B lines in the left posterior lower area and A lines disappeared. Small patchy lesions were observed, and the pleural line was discontinuous (red arrow).

Figure 7

Figure 7 & 8: The same patient. HRCT showed ground glass opacity under the pleura in the posterior upper field of the right lung. Linear array probe showed two B lines in the right posterior upper area. The pleura was depressed and unsmooth (red arrow).

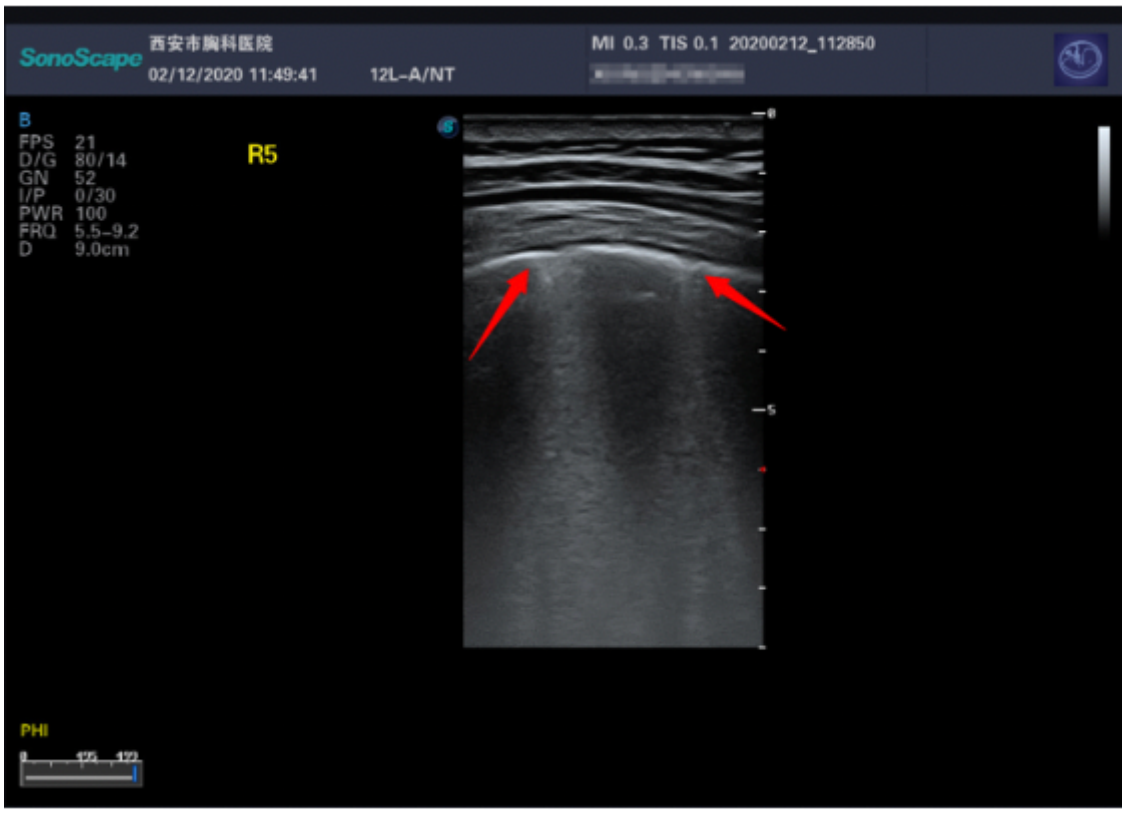

Figure 8

Figure 7 & 8: The same patient. HRCT showed ground glass opacity under the pleura in the posterior upper field of the right lung. Linear array probe showed two B lines in the right posterior upper area. The pleura was depressed and unsmooth (red arrow).

Figure 9

Figure 9 &10: The same patient. HRCT showed ground glass opacity under the pleura in the posterior basal segment of the lower lobe of the right lung, in which air bronchogram sign was visible. The linear array probe showed that the local pleural line in the right posterior lower area was unsmooth and crazy-paving pattern, and the roughness was discontinuous.

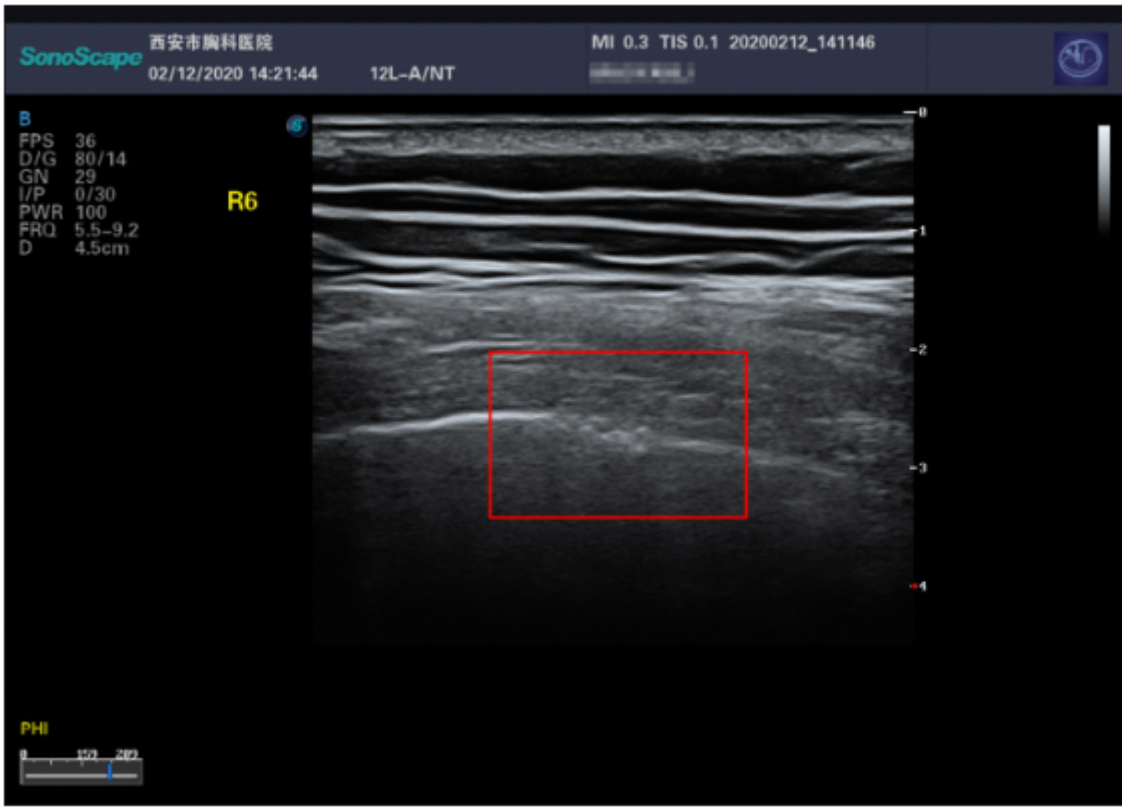

Figure 10

Figure 9 &10: The same patient. HRCT showed ground glass opacity under the pleura in the posterior basal segment of the lower lobe of the right lung, in which air bronchogram sign was visible. The linear array probe showed that the local pleural line in the right posterior lower area was unsmooth and crazy-paving pattern, and the roughness was discontinuous.

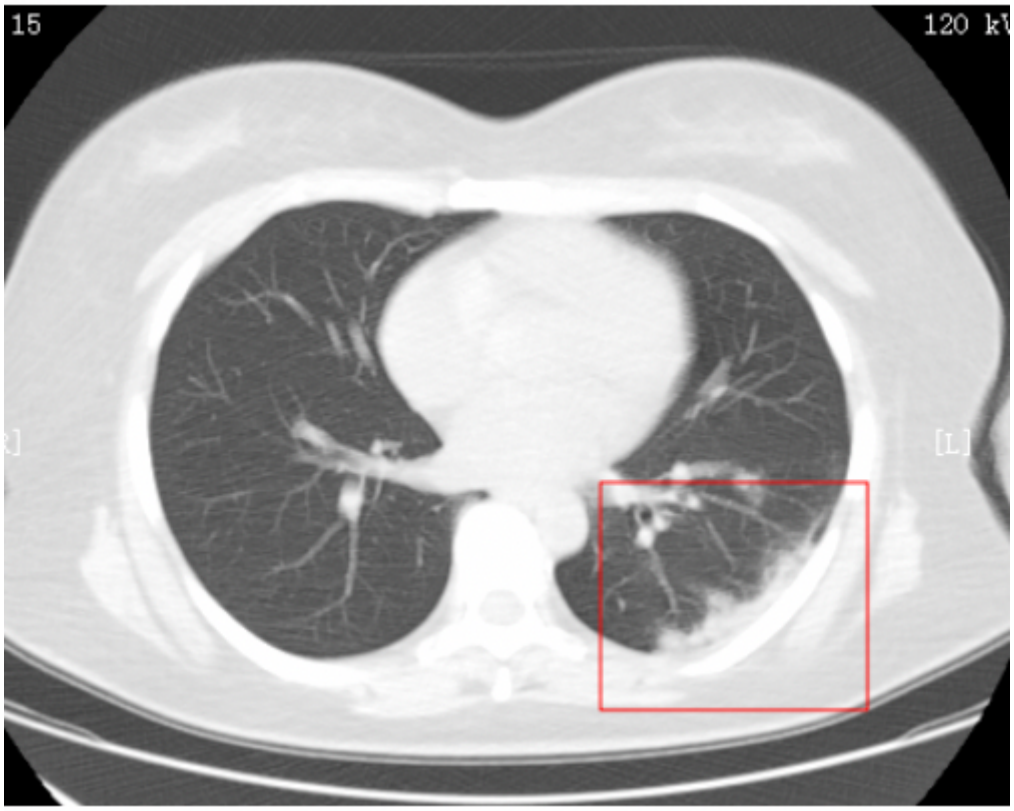

Figure 11

Figure 11 &12: The same patient. HRCT showed strip shadow under the pleura in dorsal segment of the lower lobe of the left lung. The linear array probe showed the pleural line in the left posterior upper area was interrupted and discontinuous.

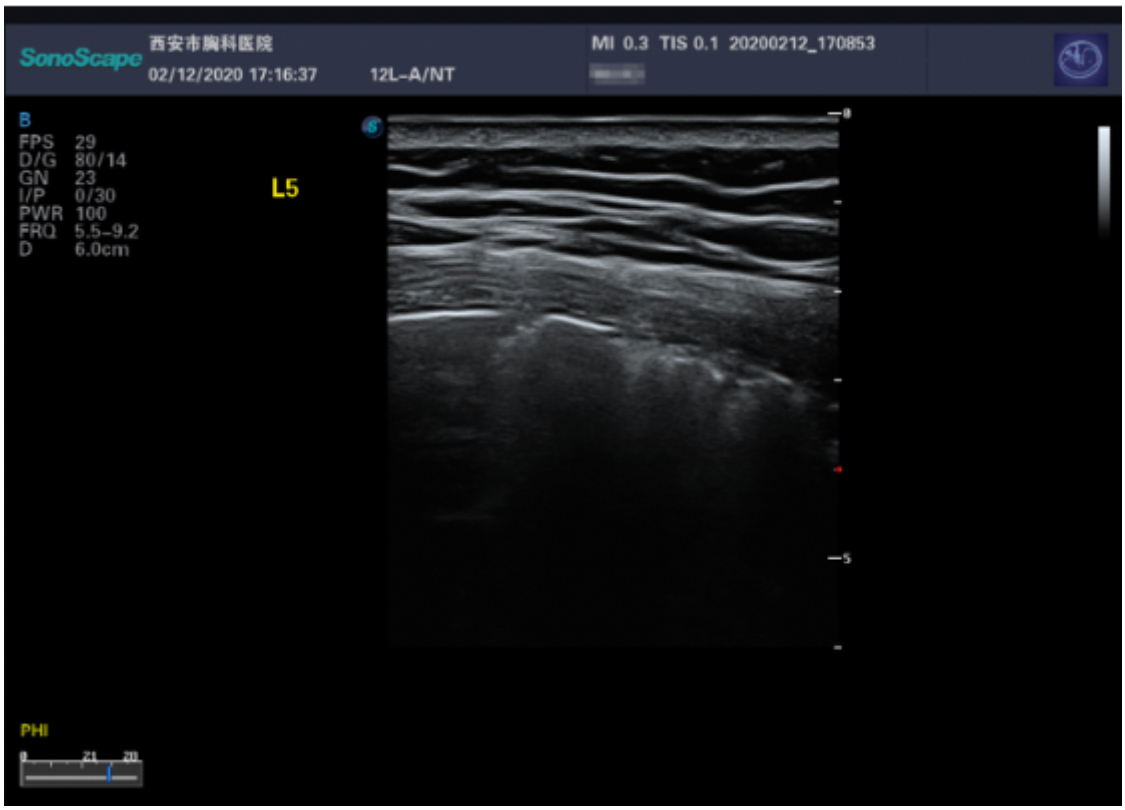

Figure 12

Figure 11 &12: The same patient. HRCT showed strip shadow under the pleura in dorsal segment of the lower lobe of the left lung. The linear array probe showed the pleural line in the left posterior upper area was interrupted and discontinuous.

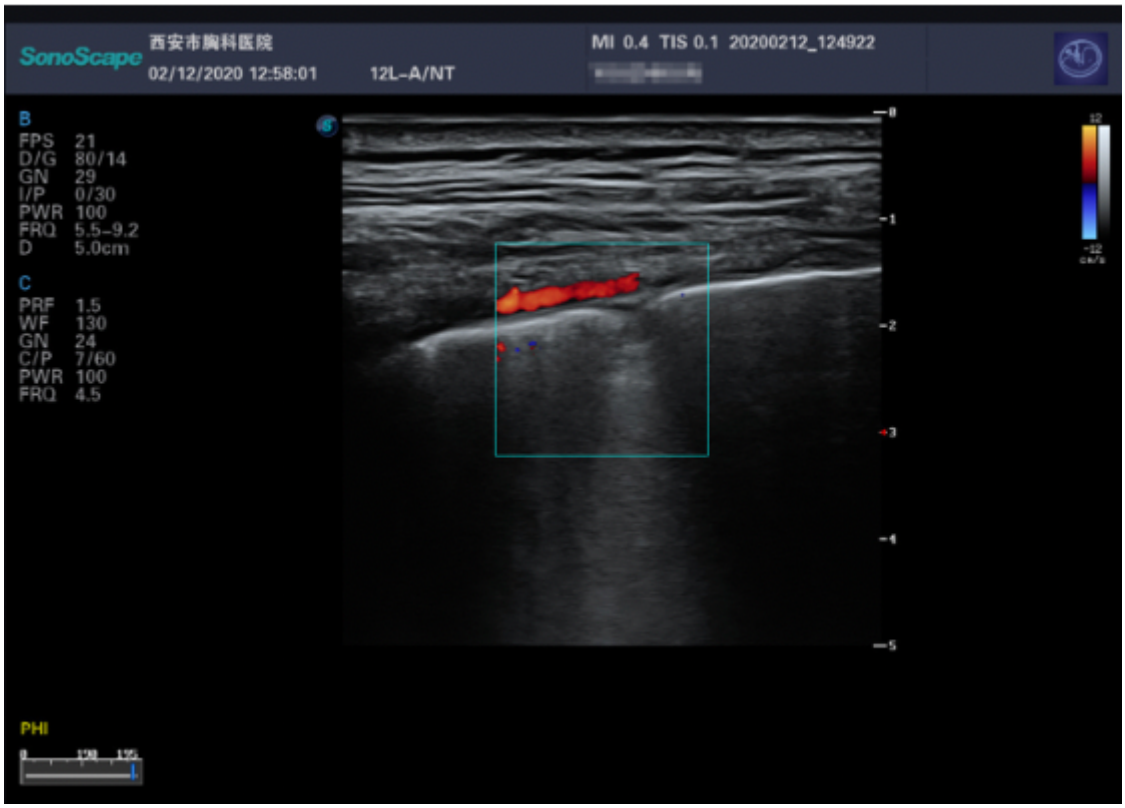

Figure 13

Figure 13: The linear array probe showed interrupted pleural line and patchy consolidation in the left posterior lower area, with fixed B lines. The origination point was round and dull, and the subpleural pleural was thickened. CDFI showed no blood flow signal.

Figure 14

Figure 14 & 15 &16: The same patient. HRCT showed patchy subpleural consolidation and air bronchogram sign in the posterior upper field of the right lung. The linear array probe showed the pleural line in the right posterior upper area was interrupted and disappeared. There was air bronchogram sign in the strip faint consolidation, and the connecting surface of the lung tissues was rough and unsmooth with B lines.

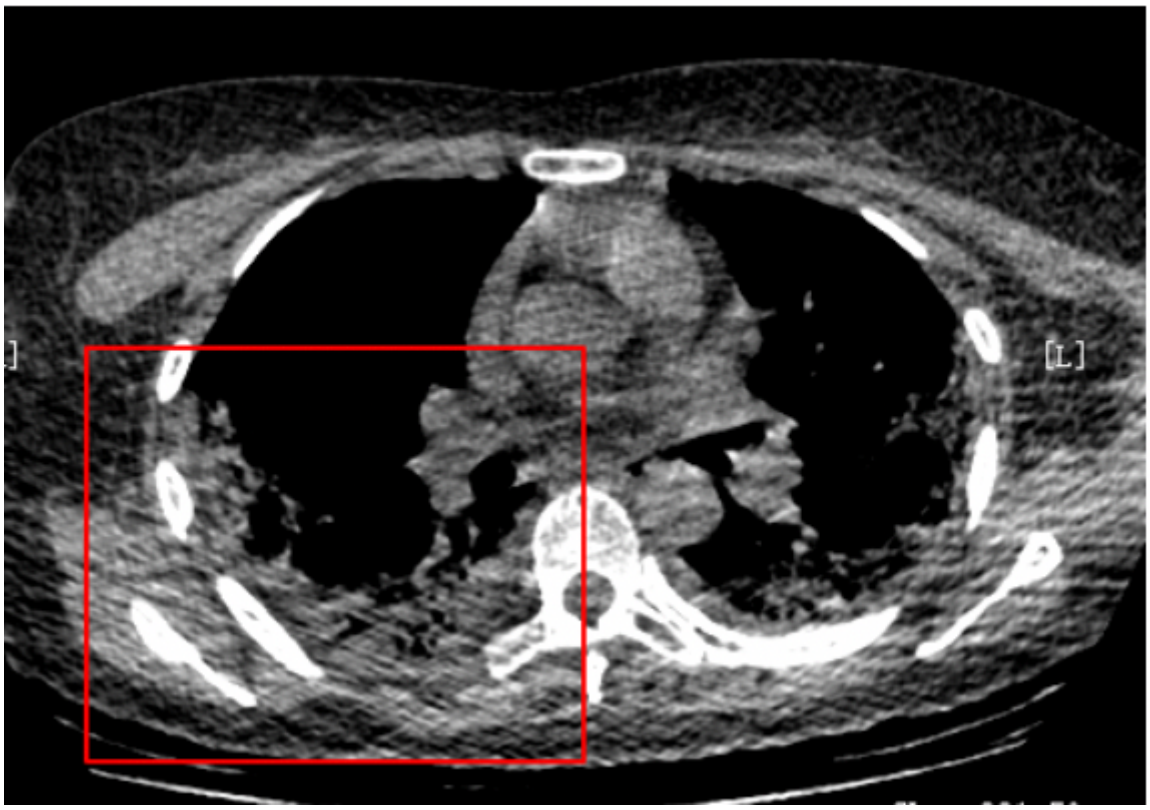

Figure 15

Figure 14 & 15 &16: The same patient. HRCT showed patchy subpleural consolidation and air bronchogram sign in the posterior upper field of the right lung. The linear array probe showed the pleural line in the right posterior upper area was interrupted and disappeared. There was air bronchogram sign in the strip faint consolidation, and the connecting surface of the lung tissues was rough and unsmooth with B lines.

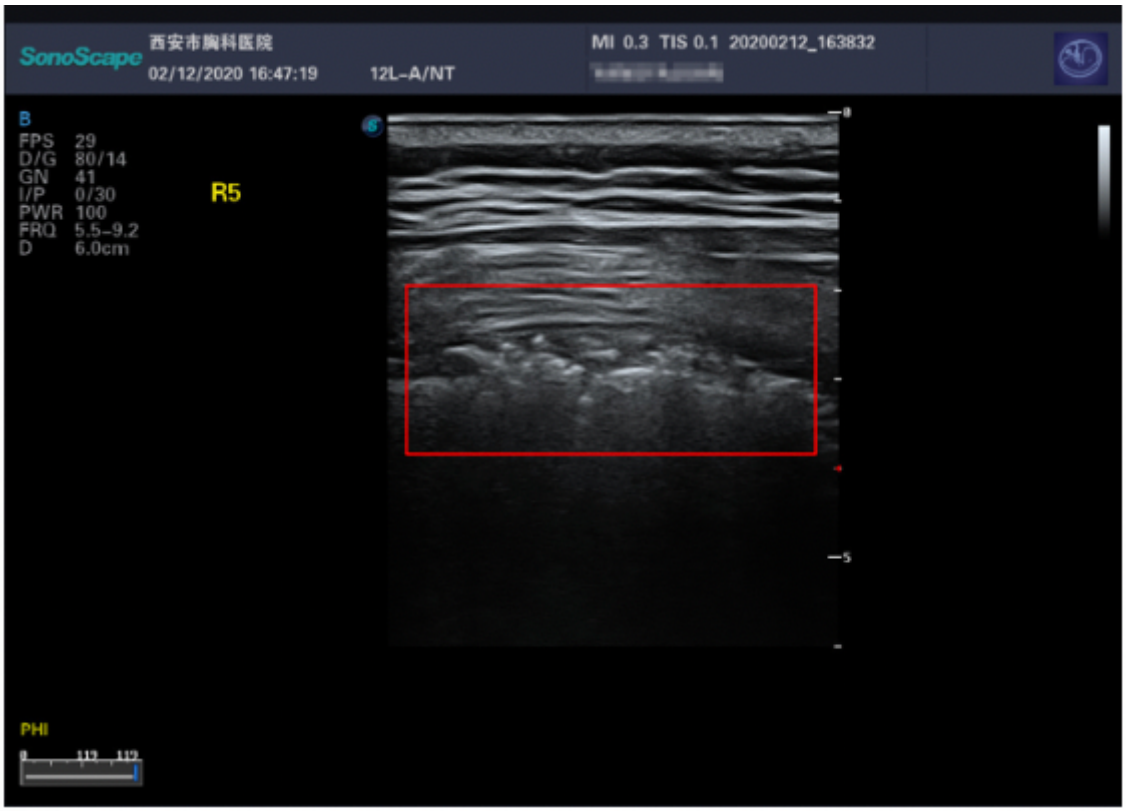

Figure 16

Figure 14 & 15 &16: The same patient. HRCT showed patchy subpleural consolidation and air bronchogram sign in the posterior upper field of the right lung. The linear array probe showed the pleural line in the right posterior upper area was interrupted and disappeared. There was air bronchogram sign in the strip faint consolidation, and the connecting surface of the lung tissues was rough and unsmooth with B lines.

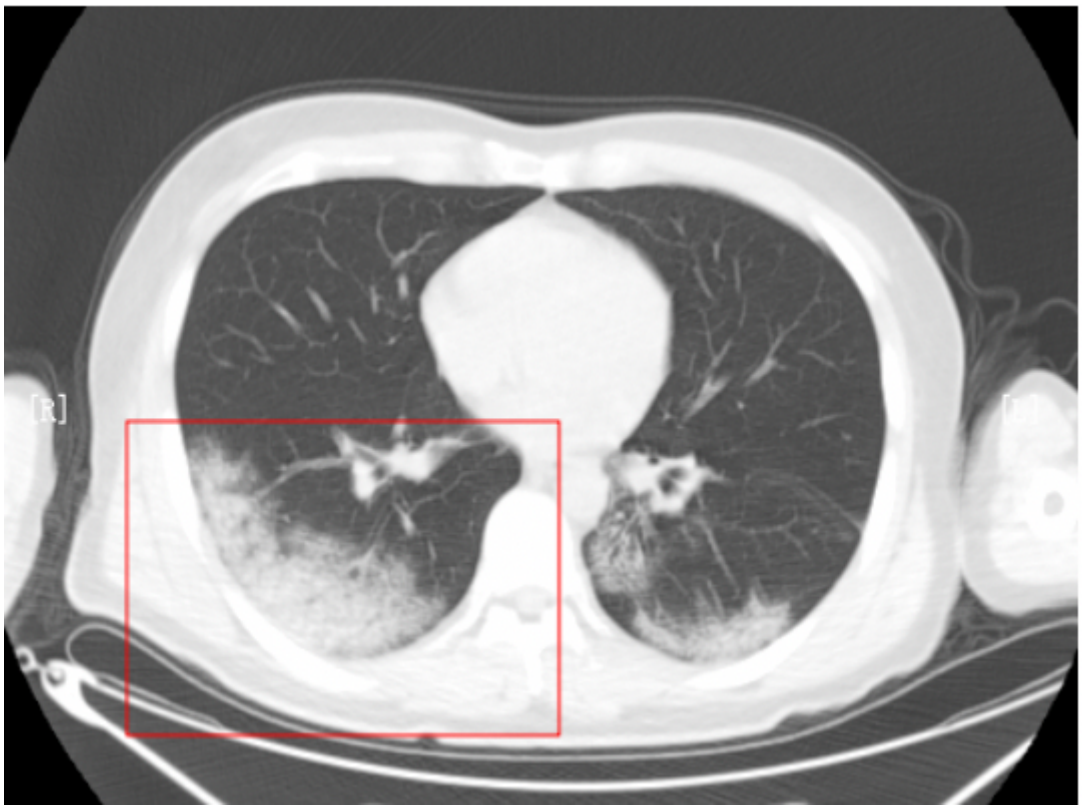

Figure 17

Figure 17-19: The same patient. HRCT showed large patchy reticular softening lesions under the pleura in the posterior basal segment of the lower lobe of the right lung. Linear array probe showed discontinuous pleural line in the right posterior lower area and strip consolidation, air bronchogram sign, crazy-paving pattern, and significant signs of interstitial disease, with a large number of B lines.

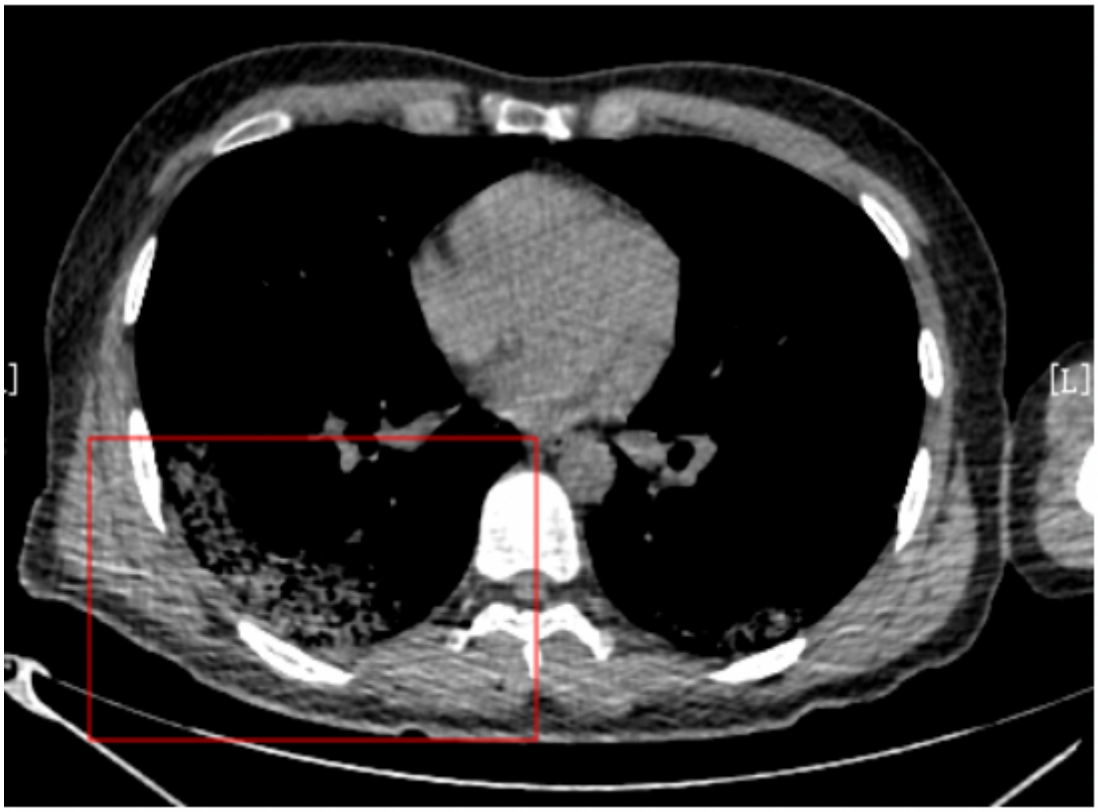

Figure 18

Figure 17-19: The same patient. HRCT showed large patchy reticular softening lesions under the pleura in the posterior basal segment of the lower lobe of the right lung. Linear array probe showed discontinuous pleural line in the right posterior lower area and strip consolidation, air bronchogram sign, crazy-paving pattern, and significant signs of interstitial disease, with a large number of B lines.

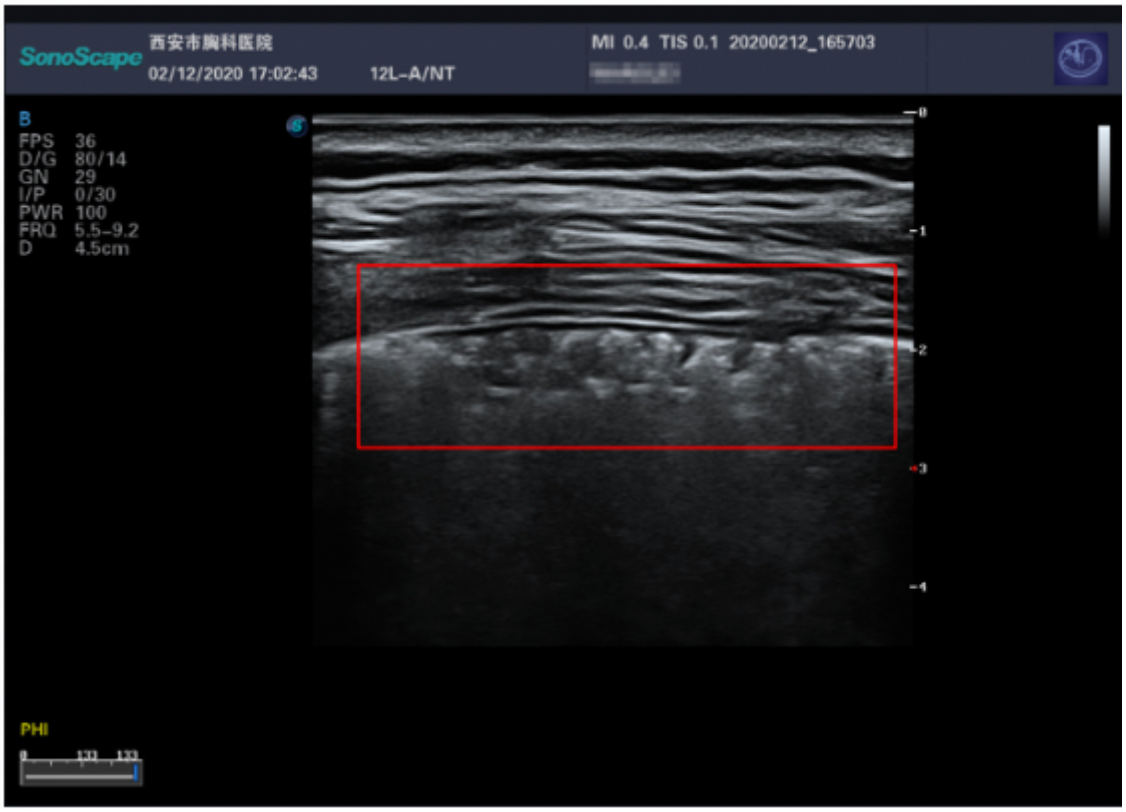

Figure 19

Figure 17-19: The same patient. HRCT showed large patchy reticular softening lesions under the pleura in the posterior basal segment of the lower lobe of the right lung. Linear array probe showed discontinuous pleural line in the right posterior lower area and strip consolidation, air bronchogram sign, crazy-paving pattern, and significant signs of interstitial disease, with a large number of B lines.

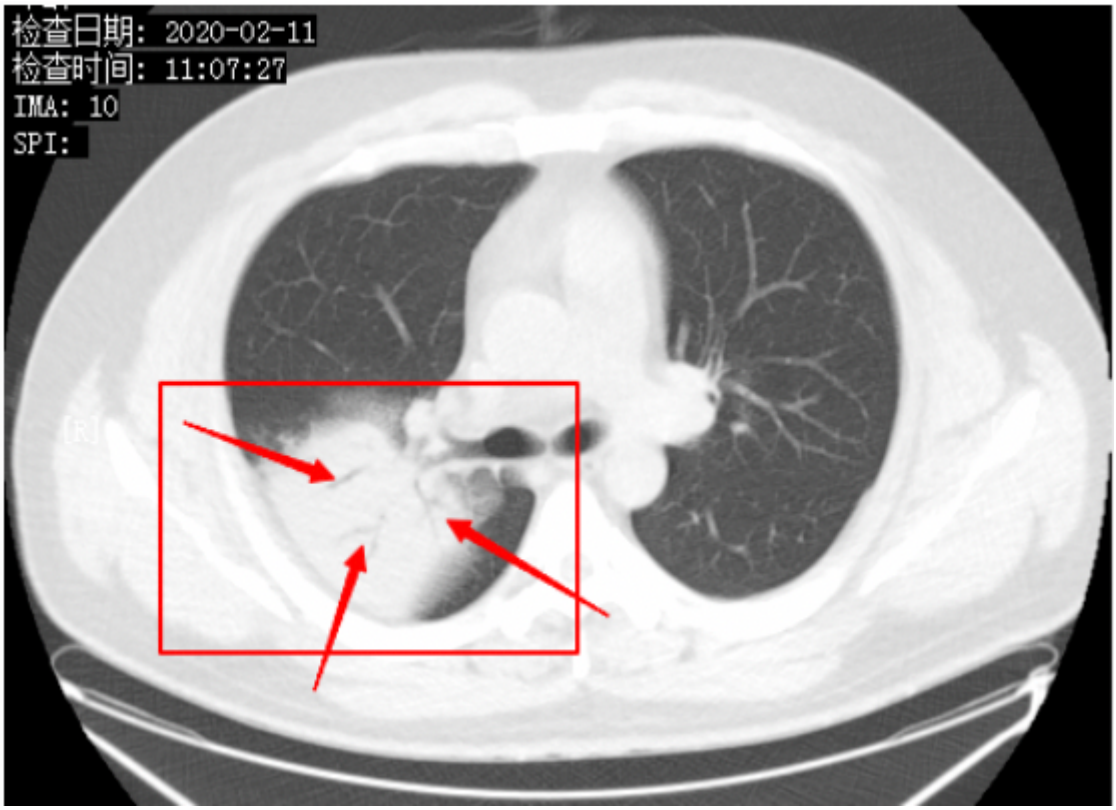

Figure 20

Figure 20-22: The same patient. HRCT showed large flaps of soft tissues and low-density shadows under the pleura in the posterior segment of upper lobe of the right lung, and large air bronchogram sign (red arrow). Convex array probe showed large areas of consolidation in the right posterior upper area and air bronchiologram sign (yellow arrow). The pleural line was interrupted.

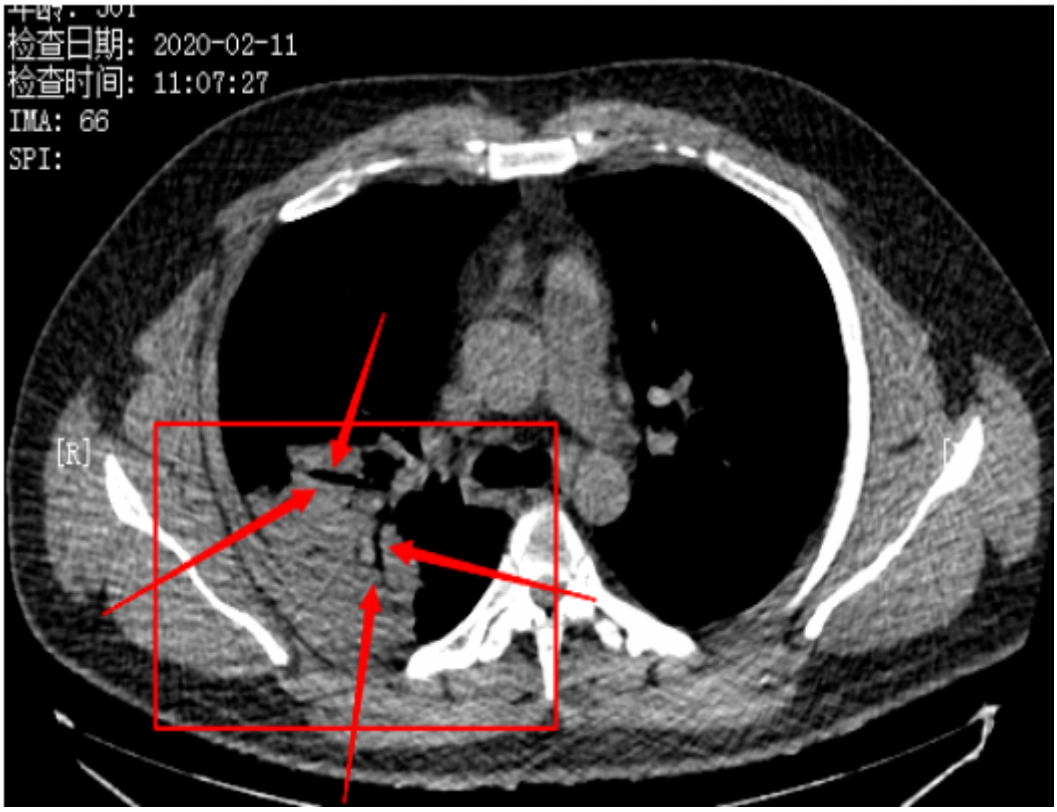

Figure 21

Figure 20-22: The same patient. HRCT showed large flaps of soft tissues and low-density shadows under the pleura in the posterior segment of upper lobe of the right lung, and large air bronchogram sign (red arrow). Convex array probe showed large areas of consolidation in the right posterior upper area and air bronchiologram sign (yellow arrow). The pleural line was interrupted.

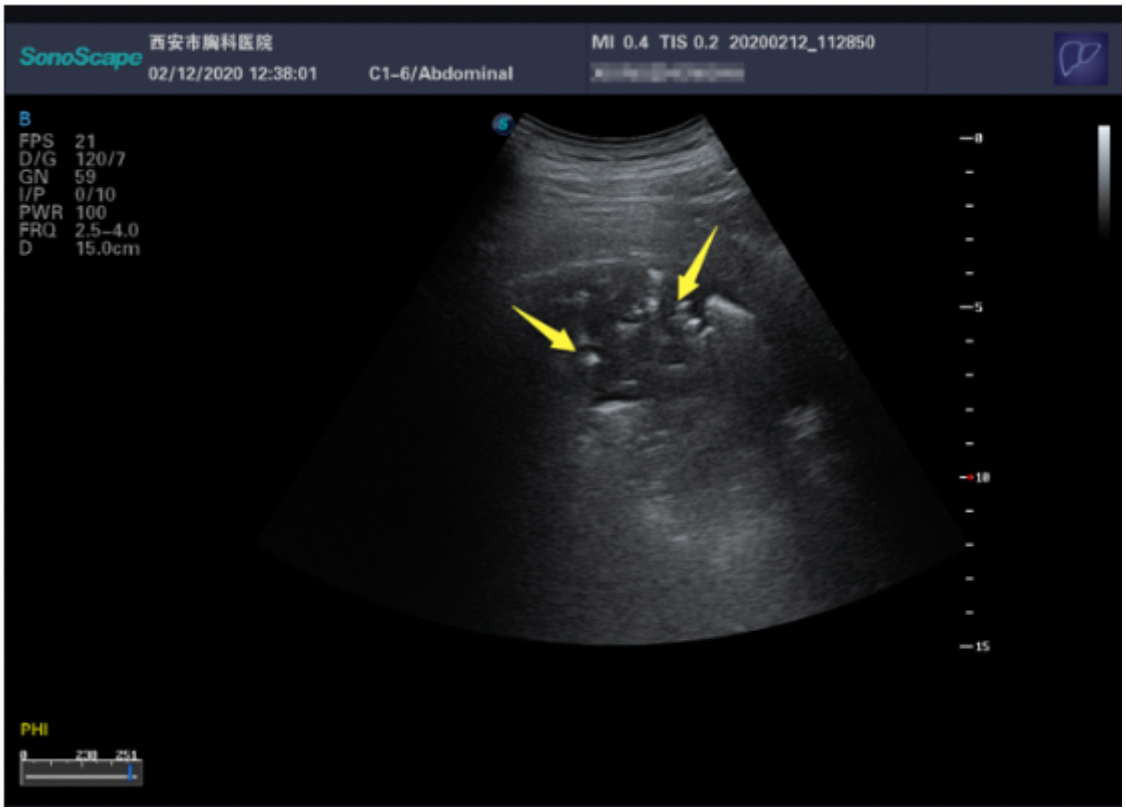

Figure 22

Figure 20-22: The same patient. HRCT showed large flaps of soft tissues and low-density shadows under the pleura in the posterior segment of upper lobe of the right lung, and large air bronchogram sign (red arrow). Convex array probe showed large areas of consolidation in the right posterior upper area and air bronchiologram sign (yellow arrow). The pleural line was interrupted.

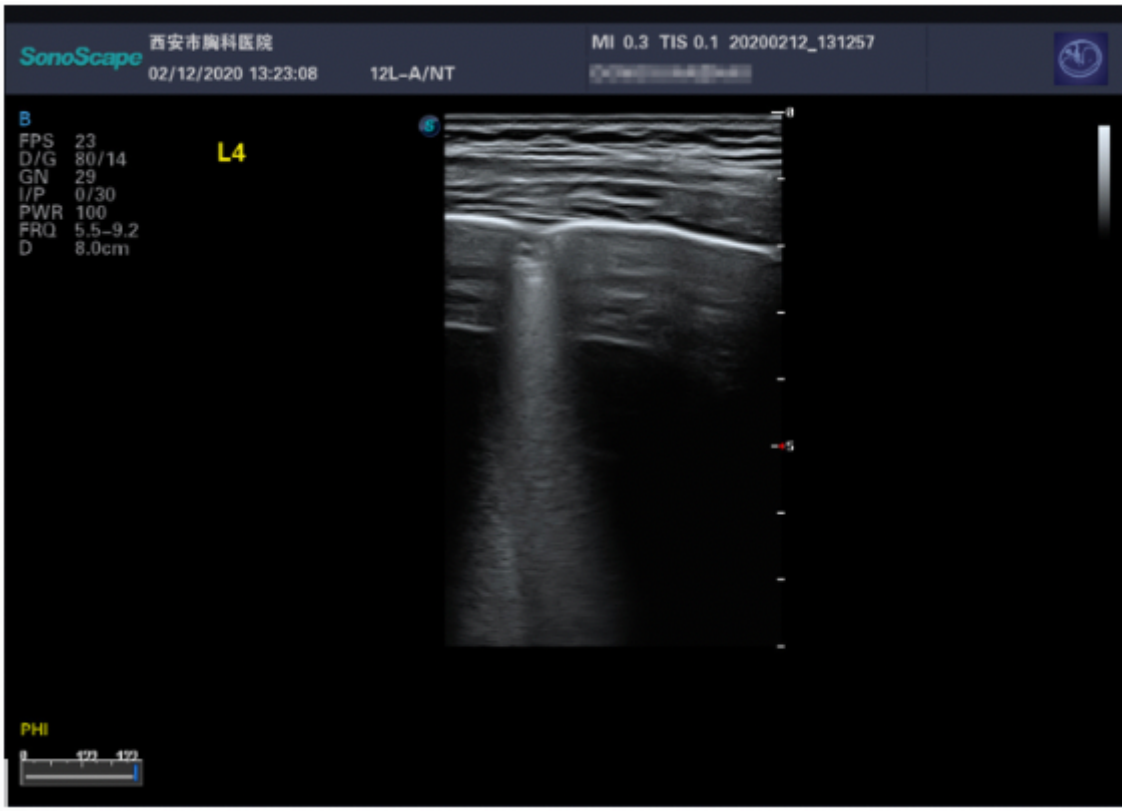

Figure 23

Figure 23: The linear array probe showed subpleural nodular irregular echo shadow in the left subaxillary field, with fixed fusion of thick B lines.

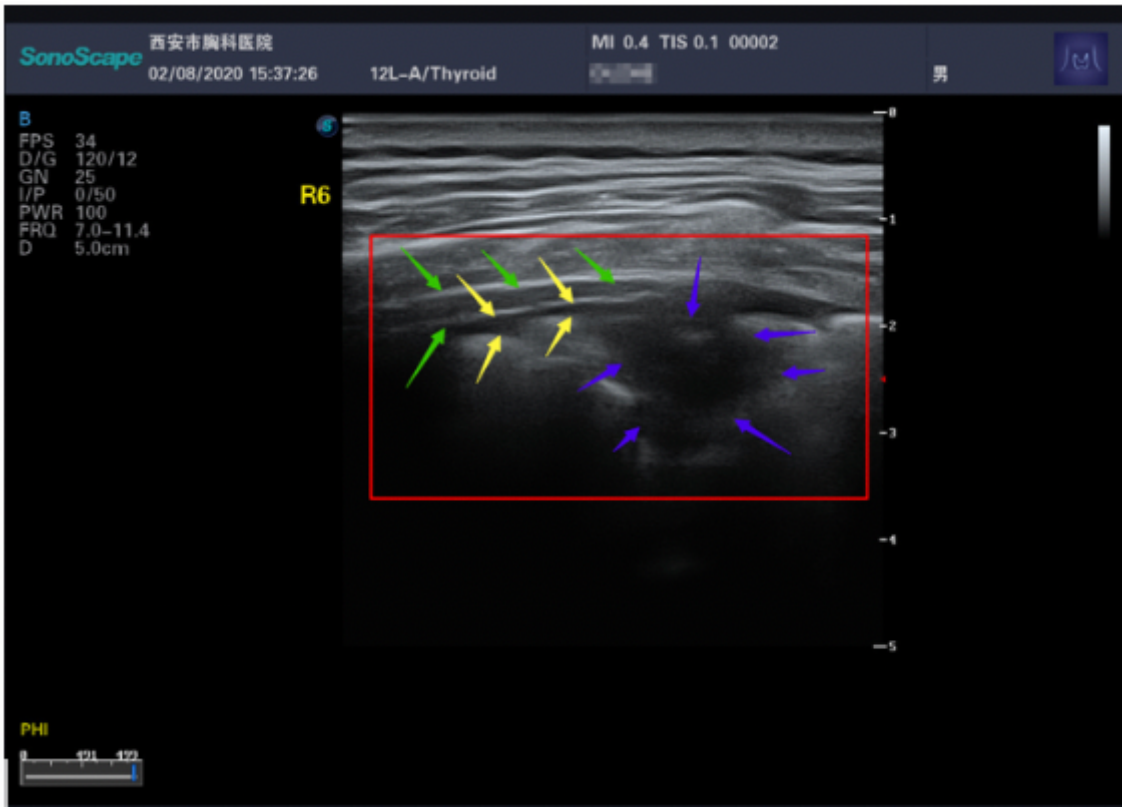

Figure 24

Figure 24: The linear array probe showed subpleural lesion with localized pleural thickening (green arrow) and localized pleural effusion (yellow arrow) in the right posterior lower area (blue arrow).

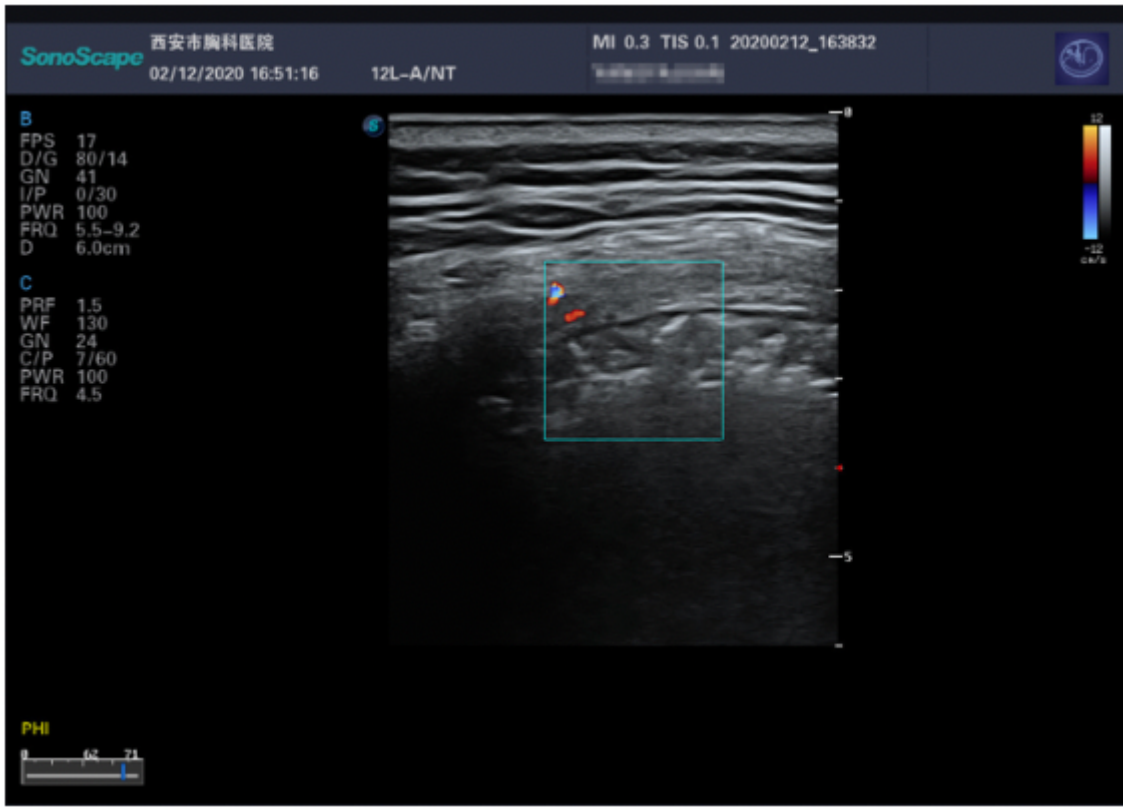

Figure 25

Figure 25: Color Doppler ultrasound showed no obvious blood flow signal in the peripulmonary consolidation of the left posterior upper area, which was significantly different from that of common inflammatory bacterial pneumonia.

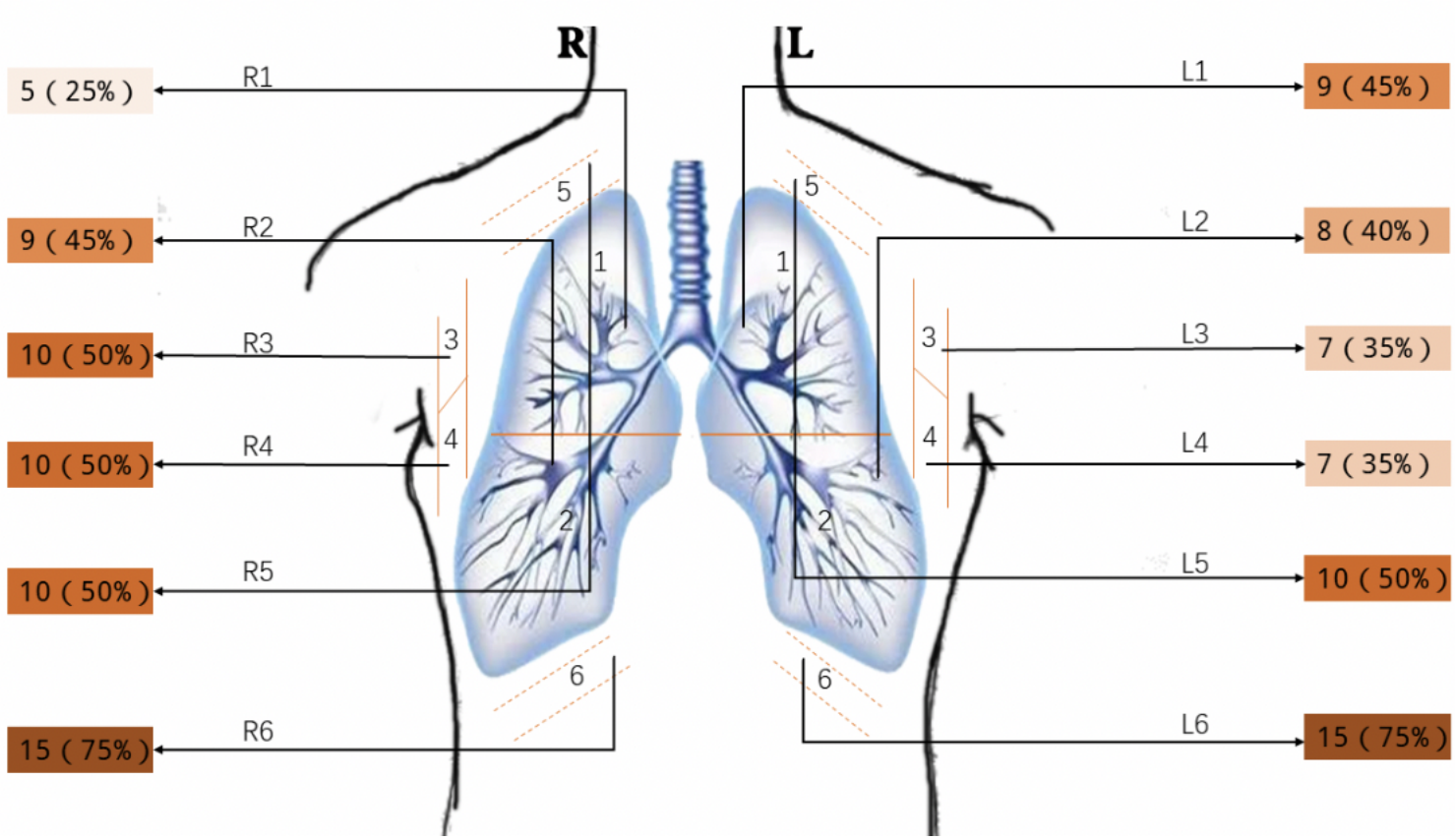

Figure 26

Diagram 1 Number of lesions in different lung areas.

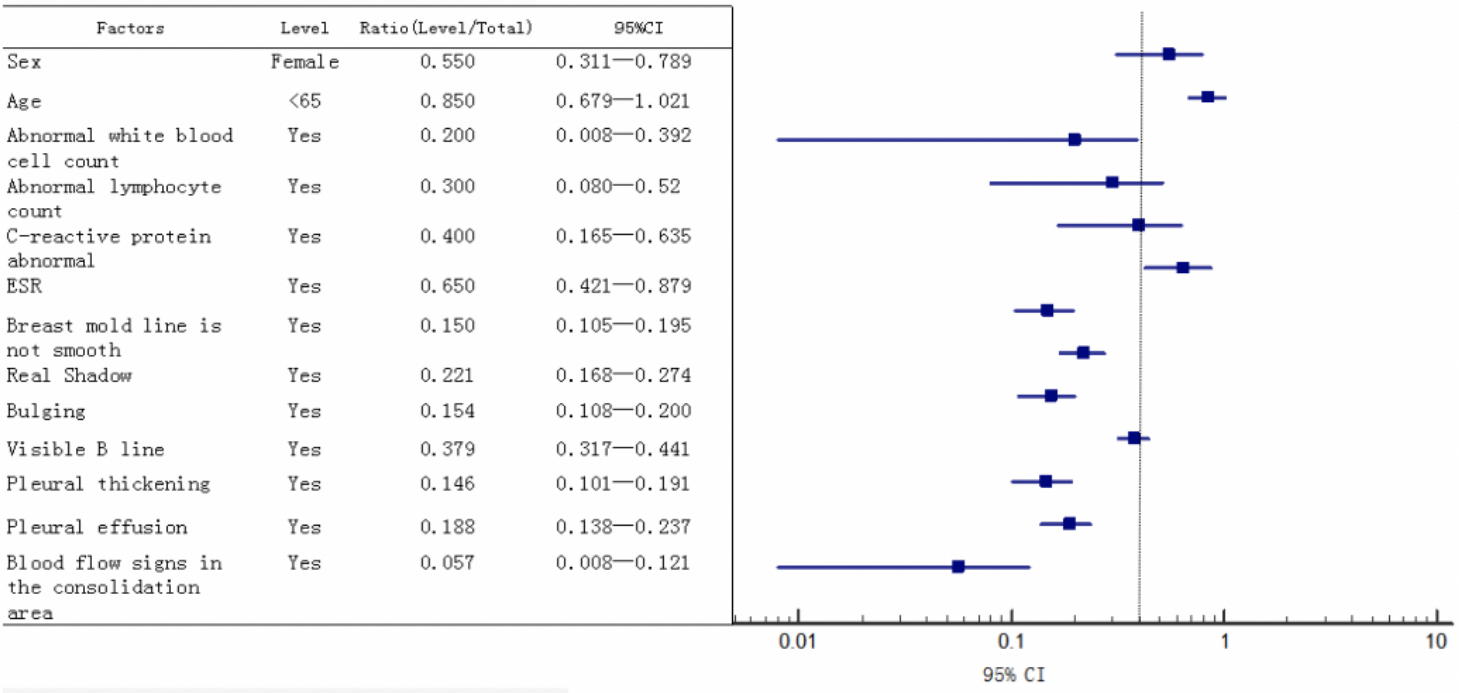

Factors	Level	Ratio(Level/Total)	95%CI
Sex	Female	0.550	0.311—0.789
Age	<65	0.850	0.679—1.021
Abnormal white blood cell count	Yes	0.200	0.008—0.392
Abnormal lymphocyte count	Yes	0.300	0.080—0.52
C-reactive protein abnormal	Yes	0.400	0.165—0.635
ESR	Yes	0.650	0.421—0.879
Breast mold line is not smooth	Yes	0.150	0.105—0.195
Real Shadow	Yes	0.221	0.168—0.274
Bulging	Yes	0.154	0.108—0.200
Visible B line	Yes	0.379	0.317—0.441
Pleural thickening	Yes	0.146	0.101—0.191
Pleural effusion	Yes	0.188	0.138—0.237
Blood flow signs in the consolidation area	Yes	0.057	0.008—0.121

Figure 27

Diagram 2 General information and ultrasonic manifestations of COVID-19.